一粗糙峰和剛性平板的原子和有限元素接觸分析
Atomistic and Finite Element Contact Analysis of an Asperity and a Rigid Plate

譚仲明[1]，張博翔[2]，陳建安[2]

[1] 光機電暨材料研究所
[2] 吳鳳科技大學

摘要

使用彈性-塑性的有限元素法和原子模擬分析一個可變形的球面與一剛性平板的無摩擦接觸。我們使用了兩種不同的方法模擬彈性-塑性接觸時的變形演變，模擬的結果發現，在使用兩種不同的模擬分析下變形機制是完全不同的，在原子模擬看到之物理現象“jump-to-contact”和“force drops during dislocation emission”我們無法在連續體的模擬中觀察到。

關鍵詞：粗糙峰，接觸，原子模擬，有限元素分析。

Abstract

The elastic-plastic finite element and atomistic models for the frictionless contact of a deformable sphere pressed by a rigid plate is presented. The evolution of the elastic-plastic contact with increasing interference is analyzed using two different analysis tools. The simulation results show that deformation mechanisms revealed in the two different analysis tools are quite different from each other. The physical phenomena “jump-to-contact” and “force drops during dislocation emission” are observed in our atomistic simulations which can not be seen in the continuum analysis.

Keywords: asperity, contact, atomistic simulation, finite element analysis.

1. INTRODUCTION

In practice, engineering surfaces are not ideally flat, but contain multiple asperities, which give the surface an uneven profile. The load between two contact surfaces is carried by the contact junctions. Thus, for two surfaces in contact, the real contact area is given not by the surface areas of the two contacting bodies, but by the sum of the contact areas of the individual asperity contact pairs. The real contact area plays a significant role in many contact problems, including those relating to friction, wear, electrical and thermal conductance, and so on. Therefore, developing a fundamental understanding of the evolution of the real contact area under the application of a load is essential in advancing the contact mechanics and many engineering applications. Packer and Hatch [1] performed an experimental investigation into the contact area between hemispherical lead specimens and a glass flat and showed that the contact area increased under tangential loading until the inception of gross sliding. McFarlane and Tabor [2] evaluated the contact area between a steel ball and an indium flat under different preloads by measuring the adhesion force between them. The results showed that under ambient conditions, the contact area increased by a factor of approximately 14 times compared to its original value under normal preload conditions. Courtney-Pratt and Eisner [3] evaluated the change in contact area between a spherically ended cone and a plate under

various normal preloads from 0.2mN to 100N by measuring the electrical conductance at the contact interface. Tabor [4] introduced the concept of "lateral junction growth" to describe the increase in the contact area produced by an increasing tangential load. The publication of Tabor's seminal study in 1959 spurred many experimental and theoretical investigations into various aspects of the junction growth phenomenon. For example, Popelar [5] studied the junction growth of a rigid perfectly-plastic two -dimensional wedge in contact with a hard smooth flat, and showed that the results were in good agreement with the experimental findings presented in [3]. Brizmer et al. [6] performed finite element analysis (FEA) simulations of an elastic-plastic preloaded spherical contact subjected to an additional tangential loading under both low and high values of the dimensionless normal load. The theoretical results obtained under high normal loads were subsequently verified by the experimental results presented by Ovcharenko et al. [7]. However, at lower values of the normal load, a noticeable difference was observed between the two sets of results. Ovcharenko et al. [7] argued that the difference between the theoretical and experimental findings was most likely the effect of surface roughness under small values of the applied load. This assertion was recently substantiated by Cohen et al. [8] who utilizing the continuum approach to evaluate the effect of surface roughness of flat on the junction growth under small normal loads. The continuing drive toward device miniaturization fueled by the evolution of new nanotechnologies renders the understanding of interfacial phenomena at the nanoscale a pivotal issue. The suitability of molecular dynamics (MD) simulations for exploring problems at the nanoscale has been demonstrated in many studies. For example, Luan and Robbins performed MD simulations to examine the validity of continuum contact mechanics at the nanoscale for contact pairs with [9] and without [10] adhesion, respectively. Meanwhile, Jeng et al. [11] applied an atomistic methodology to examine the full range of asperity contact behavior. The results were shown to be in good agreement with those predicted by continuum theory in the elastic, elastic-plastic and plastic regimes. The MD simulation results presented by Cha et al. [12] for a single asperity contact showed that the force-displacement relationship was characterized by a sawtooth-like profile due to the repetitive generation and motion of partial dislocations.

In this article we conduct finite element and atomistic simulations to explore the evolution of elastic-plastic deformation and its mechanism of the contact between an asperity and a rigid plate in both micrometer and nanometer regimes.

2. Finite element and atomistic models

2.1 Finite element model

The simulated system configurations include a rigid plate and a two-dimensional slab of copper with a single asperity at the height of 15 μm as shown in Figure 1.

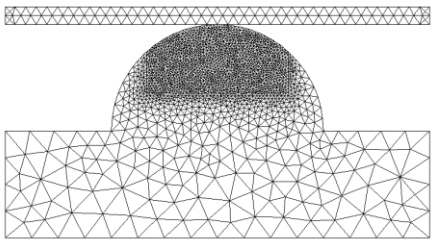

Fig. 1. Finite element model of a rigid plate and an asperity of 15 μm radius.

A commercial COMSOL 3.4 package was used to solve the contact problem. The material of the asperity was assumed elastic-plastic with identical behavior in tension and compression. Although the model can easily accommodate isotropic hardening the simpler kinematic one was selected to allow comparison with existing previous models. A static,

small-deformation analysis type was used and justified by comparison with the results of a large-deformation analysis. The von Mises yielding criterion was used to detect the onset from elastic to elastic-plastic deformation. The finite element method numerical solution requires as an input some specific material properties such as the Young's Modulus and poisson's ratio.

2.2 Atomistic model

Figure 2 presents the simulation model employed to investigate the contact of a perfect copper asperity and a rigid plate. In order that deformation of the plate may be ignored within the simulation, an assumption is made that the elastic modulus of the plate is much greater than the one of the copper asperity. Furthermore, a boundary condition is imposed which assumes that the atoms at the base of the copper slab are fully constrained. The dimensions of the simulated copper slab are 600 $^{\circ}_{A}$ x150 $^{\circ}_{A}$ and the radius of the asperity is 150 $^{\circ}_{A}$.

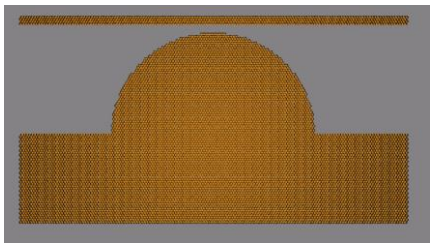

Fig. 2. Atomistic model of a rigid plate and an asperity of 150 $^{\circ}_{A}$ radius.

The Morse potential is employed to model the interatomic pairwise potentials of the copper asperity. This potential function is given by:

$$\phi(r_{ij}) = D\{\exp[-2\alpha(r_{ij} - r_0)] - 2\exp[-\alpha(r_{ij} - r_0)]\} \quad (1)$$

where rij is the distance between atoms i and j, and the copper constants D, α, and ro are specified as 0.3429, 0.9545, and 2.7202, respectively. Furthermore, the simulation adopts the Born-Mayer potential to model the interactions between the plate and the copper atoms. This potential generates an impulsive force only, and is expressed as:

$$\phi(r_{ij}) = A\exp[-2\alpha(r_{ij} - r_0)] \quad (2)$$

where rij is the distance between plate atom i and copper atom j, and the plate/copper constants A, a, and ro are taken to be 0.3579 eV, 0.9545 1/$^{\circ}_{A}$, and 2.5 $^{\circ}_{A}$, respectively. A computationally efficient approach based on the nonlinear finite element formulation is established by taking any two arbitrary atoms i and j as two nodes, and their potential as one element. It is assumed that the coordinates of atom i are (x i ,y i ,zi) and that its displacements in the x-. y- and z-directions are given by u i , v i and wi , respectively. By defining the nodal displacement vector, {u}i j , and the corresponding external nodal force vector, {F}i j =(f i, g i , hi , f j , g j , hj) T , for atoms i and j , the total pairwise potential energy can be expressed in the form of:

$$E_{ij} = \phi(r_{ij}) - \{u\}_{ij}^{T}\{F\}_{ij} \quad (3)$$

where the atomic distance, ri j , is given by:

$$r_{ij} = \left\{(x_i + u_i - x_j - u_j)^2 + (y_i + v_i - y_j - v_j)^2 + (z_i + w_i - z_j - w_j)^2\right\}^{1/2} \quad (4)$$

Such that its differential with respect to $\{u\}_{i\,j}$ is:

$$dr_{ij} = [B]d\{u\}_{ij} \quad (5)$$

Applying the principle of minimum work enforces the minimization of E_{ij} with respect to $\{u\}_{ij}$, i.e.

$$\frac{\partial E_{ij}}{\partial \{u\}_{ij}} = \left(\frac{\partial \phi}{\partial r_{ij}}\right)[B]^T - \{F\}_{ij} = \{0\} \tag{6}$$

It is noted that equation (6) is the element equilibrium equation and therefore represents the equilibrium of the various forces acting on atoms i and j. An unbalanced force, $\{\xi\}ij$, can be defined in the form of :

$$\{\xi\}_{ij} = \left(\frac{\partial \phi}{\partial r_{ij}}\right)[B]^T - \{F\}_{ij} \tag{7}$$

The equilibrium equation is solved by means of an iterative procedure which continues until the equation converges to zero with an acceptable tolerance. In order to solve the nonlinear equilibrium equation using an iterative procedure, it is first necessary to differentiate $\{\xi\}ij$ with respect to $\{u\}ij$, i.e.

$$\begin{aligned} d\{\xi\}_{ij} &= d\left(\frac{\partial \phi}{\partial r_{ij}}\right)[B]^T + \left(\frac{\partial \phi}{\partial r_{ij}}\right) d[B]^T \\ &= [B]^T \left(\frac{\partial^2 \phi}{\partial r_{ij}^2}\right) dr_{ij} + \left(\frac{\partial \phi}{\partial r_{ij}}\right) d[B]^T \\ &= \left([K]_{ij} + [K_\sigma]_{ij}\right) d\{u\}_{ij} \\ &= [K_T]_{ij}\, d\{u\}_{ij} \end{aligned} \tag{8}$$

where

$$[K]_{ij} = [B]^T \left(\frac{\partial^2 \phi}{\partial r_{ij}^2}\right)[B] \tag{9}$$

and

$$[K_\sigma]_{ij} = \left(\frac{\phi}{r_{ij}}\right)\left[\frac{\partial [B]^T}{\partial u_i}, \frac{\partial [B]^T}{\partial v_i}, \frac{\partial [B]^T}{\partial w_i}, \frac{\partial [B]^T}{\partial u_j}, \frac{\partial [B]^T}{\partial v_j}, \frac{\partial [B]^T}{\partial w_j}\right] \tag{10}$$

Equation (9) can be solved by substituting equation (5) into the second line of equation (8). Subsequently, the conventional assembly procedure of the finite element formulation is applied to assemble equation (8) in order to derive the total system equation, i.e.

$$d\{\xi\} = [K_T] d\{u\} \tag{11}$$

Similarly, equation (7) can be assembled to derive the total system equilibrium equation, i.e.

$$\sum_{i \neq j} \left(\frac{\partial \phi}{\partial r_{ij}}\right)[B]^T - \{F\}_{ij} = \{f\}_{\text{internal}} - \{F\}_{\text{external}} = \{0\} \tag{12}$$

In terms of the finite element formulation, equation (11) represents the tangent stiffness equation, while the terms $\{f\}_{\text{internal}}$ and $\{F\}_{external}$ in equation (12) denote the internal force vector and the external force vector, respectively. The Newton-Raphson iterative technique is applied to solve the total system equilibrium equation given in equation (12) using a suitable displacement control scheme. Once the equilibrium path of each atom has been determined, a slip vector, which is closely related to the Burgers vector, can be defined for each atom, i.e.

$$s = \frac{1}{n_s}\sum_{i=1}^{n_s} d_t^i - d_\theta^i \qquad (13)$$

where i refers to the nearest neighbors of the atom in question, n_s refers to the number of neighboring atoms which have slipped, and d_t^i and d_θ^i are vectors from the atom in question to the neighboring atom at step t and θ, respectively. Conventionally, step θ indicates the step immediately prior to indentation, i.e. the point at which zero stress has been induced by the indenter.

3.Results and discussion

Contacting process is simulated moving the plate downward incrementally to impress the copper asperity. Every time the plate moves downward a displacement increment, the energy of the whole system is minimized to achieve the equilibrium. Energy minimization algorithm used in COMSOL 3.4 is the modified Newton-Raphson method. In this study, we have simulated a whole loading-unloading cycle with respect to the copper asperity with a small displacement increment 0.1 μm. The curve of load (force experienced by the plate) versus interference are recorded as shown in the figure 3.

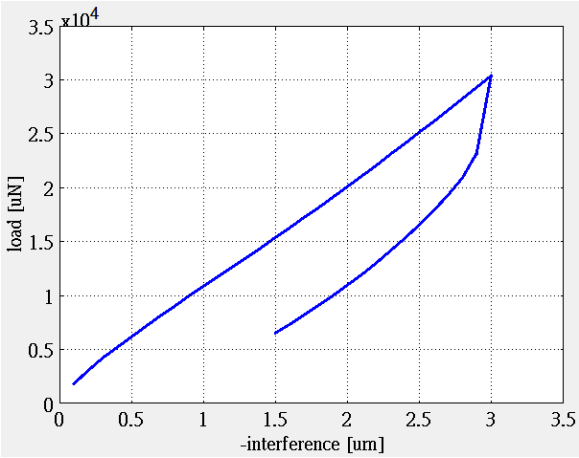

Fig. 3. The loading and unloading versus interference curve obtained from the finite element simulation.

It can be seen in figure3 that the loading and unloading cycle recorded represents hysteretic loop, i.e. there are plastic deformations occurred in the whole process. It will be obviously seen comparing with the one obtained later from the atomistic simulation that the energy dissipated in the loop is much less. In figure 4, subplots (a), (c), and (e) show the von Mises stress distributions inside the asperity at three interference values(0.3 μm, 0.6 μm, 0.9 μm). Correspondingly, subplots (b), (d), and (f) in figure 4 show the development of the plastic region at the three interference values. Because an elasto-plastic solution is load-path dependent, it is important not to use too large steps in the load parameter when you anticipate a plastic flow. Usually you can take one large step up to the elastic limit, as our simulation did. Moreover, reversed plastic flow can occur during the unloading. This is why small parameter steps are used in this analysis. The von Mises yielding criterion is adopted in the simulation. Therefore, the plastic strain takes place once the stress level of a material point reaches the yielding strength. This explains why the plastic regions in subplots (b), (d), and (f) will coincide with the ones of which von Mises stresses are larger than the yielding stress (110 MPa) in subplot (a), (c), and (e). The plastic deformation mechanism in the finite element simulation is governed by J2 plasticity theory. Consequently, the evolution of the plastic

region will be influence by the hardening rule adopted in the simulation. For copper, kinematic hardening rule is an appropriate choice.

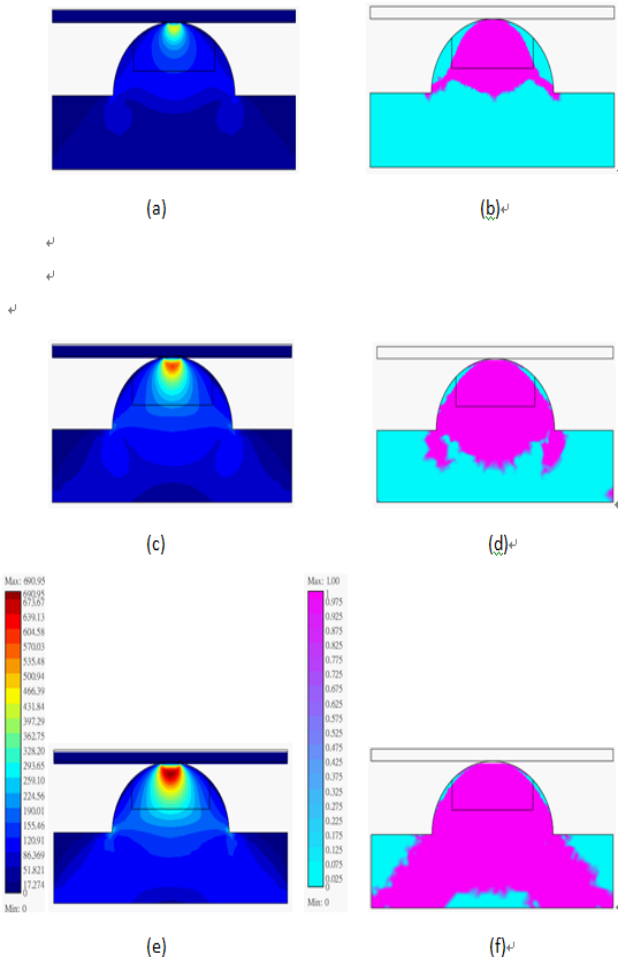

Fig. 4. von Mises stress distributions and regions of plastic deformation of copper asperity impressed by the rigid plate at three interference values.

When the size of the asperity goes down to nanometer scale, atomistic simulations are believed to be a suitable tool to investigate the underlying physics of the contact analysis of the asperity. The rigid flat was positioned at a height of 10Å above the top of the asperity and was then moved in a downward direction in an incremental manner with a displacement of 0.1Å in each step. Figure 5 presents the variation of the normal force acting on the rigid flat as a function of the displacement.

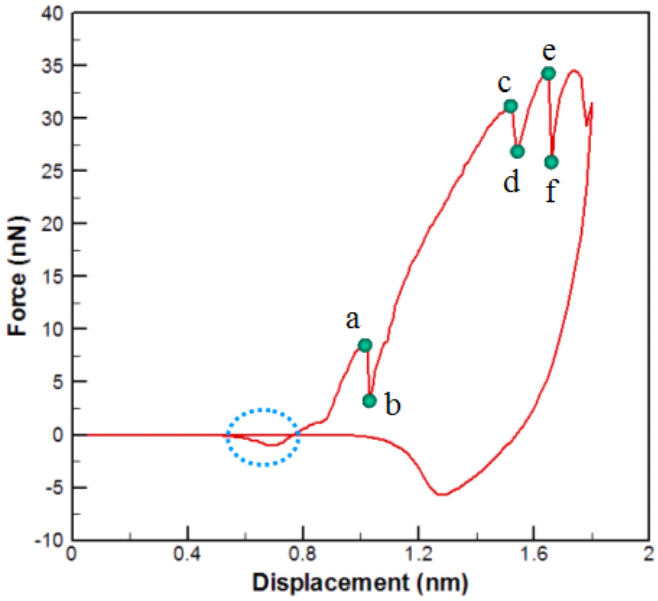

Fig. 5. The loading and unloading versus interference curve obtained from the atomistic simulation.

Note that the displacement value is measured in the vertical direction from the initial position of the flat. The simulation results obtained for the slip vector norms and von Mises stress distributions at each of the six key steps labeled in Fig. 6 (i.e. (a) ~ (f)) are shown in Fig. 5. As shown in Fig. 5, the normal force drops slightly just before the flat comes into contact with the asperity. This finding is consistent with the "jump -to-contact" phenomenon reported by Cha et al. [12] for adhesive contacts. During the loading process, the normal force increases with an increasing displacement, but experiences three intermediate drops, as indicated by labels (a-b), (c-d) and (e-f), respectively.

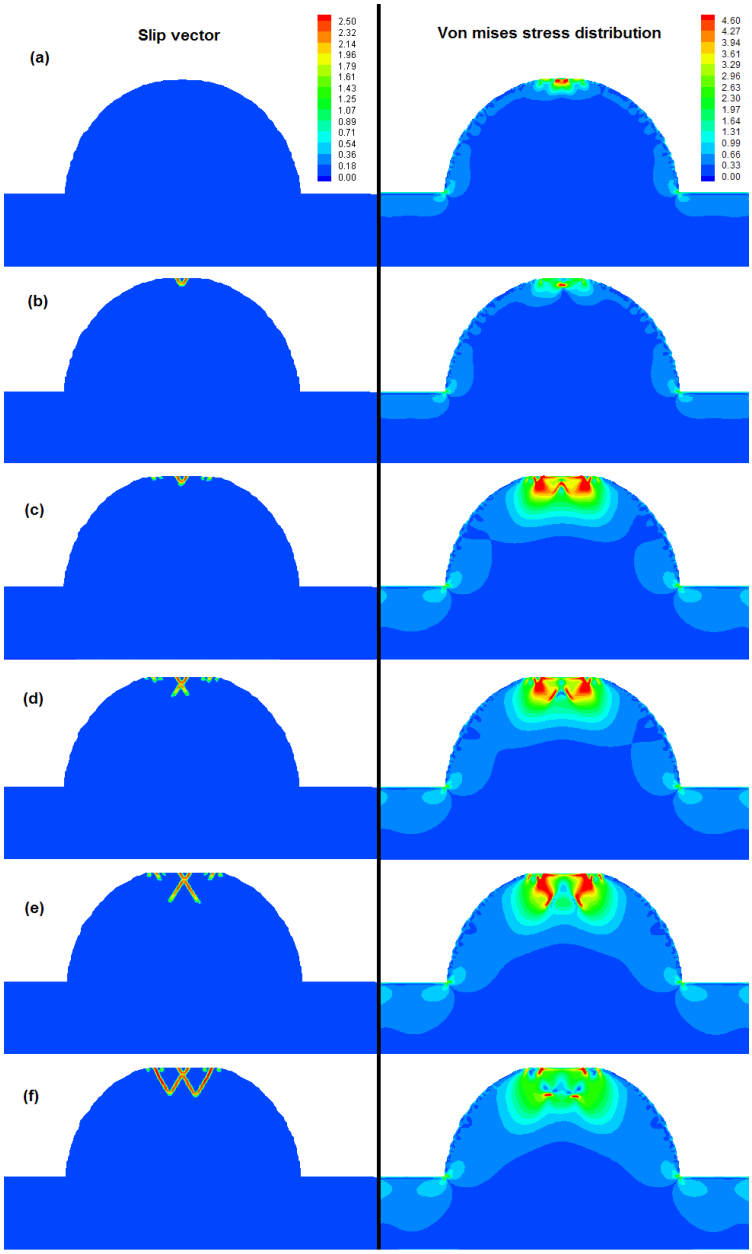

Fig. 6. Slip vector norms and von Mises stress distributions corresponding to points (a)~(f) in Fig. 5

Observing Fig. 6(a), corresponding to point (a) in Fig. 5, it can be seen that while a localized high von Mises stress exists at the top of the asperity, no obvious slips of the asperity atoms occur. However, when the flat is displaced from point (a) to point (b) in Fig. 5, the asperity atoms slip along the <211> and <12 1 > directions, as shown in Fig. 6(b). It can be seen that the intensity of the von Mises stress distribution in Fig. 6(b) is lower than that in Fig. 6(a), which indicates that the slip of the asperity atoms releases the von Mises stress and therefore results in a reduction in the force acting on the flat (see point (b) in Fig. 5). Thereafter, the continued movement of the flat in the downward direction causes the force acting on the flat to increase rapidly toward a second local maximum value, corresponding to point (c) in Fig. 5. Referring to Fig. 6, it can be seen that the von Mises stress distribution corresponding to point (c) in Fig. 5 has the form of an inverted V at the top of the asperity. This localized high von Mises stress causes the <211> and <12 1 > slip lines generated at point (b) to extend further into the asperity as the flat continues to move in the downward

direction (see Fig. 6(d)). The corresponding slip of the asperity atoms reduces the magnitude of the force acting on the flat (see point (d) in Fig. 5), but causes the neighboring atoms have a high stress. Similarly, a further displacement of the flat in the downward direction (i.e. from point (e) to point (f) in Fig. 5) causes the von Mises stress induced at point (e) to be released via a slip of the asperity atoms along the <211> and <12 1 > directions at point (f). The results presented in Figs. 5 and 6 provide direct evidence that the slip of the asperity atoms during contact is the result of the localized high von Mises stress. Furthermore, the slip of the asperity atoms leads to a release of the von Mises stress and therefore causes a drop in the force acting on the flat. Overall, the simulation results indicate that the localized high von Mises stress, the occurrence of asperity atom slips, and the force acting on the flat have an inseparable relationship.

4. Conclusion

In conclusion, we conducted atomistic and finite element simulations to do contact analysis of an asperity and a rigid plate at both micrometer and nanometer regimes. The simulation results show that deformation mechanisms revealed in the two different analysis tools are quite different from each other. It is also concluded that the energy dissipated in the loading-unloading process in the finite element analysis is much less than the corresponding results from the atomistic simulation. Moreover, the physical phenomena “jump-to-contact” and “force drops during dislocation emission” are observed in our atomistic simulations which can not be seen in the continuum analysis.

Reference

[1] R.C. Parker and D. Hatch, Proc. Phys. Soc.London, Sect. B, vol. 63, pp. 185–197, 1950.
[2] J.S. McFarlane and D. Tabor, Proc. R. Soc. Lond. A, vol.202, pp. 244–253, 1950.
[3] J.S. Courtney-Pratt and E. Eisner, Proc. R. Soc. Lond. A, vol. 238, pp. 529–550, 1957.
[4] D. Tabor, Proc. R. Soc. Lond., Ser. A., vol.251, pp. 378–393, 1959.
[5] C.H. Popelar, ASME Trans. J. Appl. Mech., vol. 36, pp.132–133, 1969.
[6] V. Brizmer, Y. Kligerman and I. Etsion, ASME J. Tribol., vol. 129, pp.783–790, 2007.
[7] A. Ovcharenko, G. Halperin and I. Etsion, Wear, vol. 264, pp. 1043–1050, 2008.
[8] D. Cohen, Y. Kligerman, and I. Etsion,Phys. Rev. E, vol. 74, pp. 026111, 2006.
[9] B.Q. Luan and M.O. Robbins, Phys. Rev. E, vol. 74, pp. 026111, 2006.
[10]B.Q. Luan and M.O. Robbins, Nature, vol. 435, pp. 929–932, 2005.
[11]Y.R. Jeng, and W.C. Kao and P.C. Tsai, Appl. Phys. Lett., vol. 91, pp. 091904, 2007.
[12]P.R. Cha, D.J. Srolovitz and T.K. Vanderlick, Acta Mater., vol. 52, pp. 3983–3996, 2004.